

# MEMS Group Project

## Analysis of a 3-Axis capacitive accelerometer

### Group 1.3

Fantini Pietro  
Giugliarelli Marco  
Vicariotto Tommaso

January 4, 2024

#### Abstract

This report aims at briefly describing the work performed in the context of the group project of the MEMS course, taught by professor Juillard. The project, regarding the reverse engineering of a 3-axis capacitive accelerometer (Project 1), was supervised by Miss Zalfa Jouni.

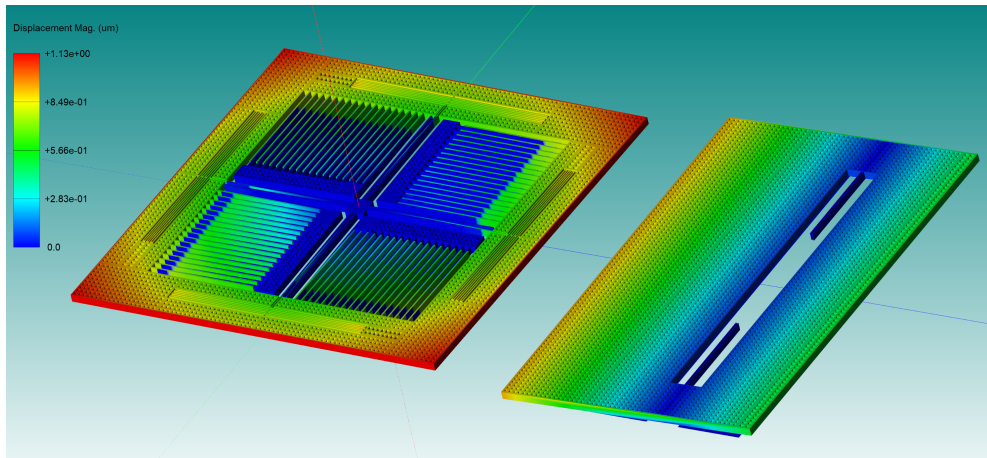


Figure 1: Our model in the modal analysis

# 1 Project introduction

Our goal was to reverse-engineer the design of a three-axis capacitive accelerometer of which three axes are integrated on the same substrate. This design choice proposes to overcome some issues of the standard approach of using three single-axis accelerometers, which are:

- Added cost of packaging.
- Larger footprint.
- Accuracy, since the axes must be precisely aligned.

The option of integrating the three axes on the same substrate has of course itself some issues. The main one is that since MEMS fabrication processes are planar processes it is difficult to achieve equal performances in the in-plane and out-of-plane directions. These results inevitably resulted in compromises that we are going to explore in this report. The accelerometer we are referring to is LIS331DLH of STMicroelectronics.

## 2 Model's Data

Our first approach was to understand the dimension of each element of the sensor. We basically exploited images (Fig. 3left and 2 found in the article [1]. As figure 3 shows a scale ( $20\mu m$ ), on a first analysis we recovered almost all the dimensions of the model, shown in figure 5.

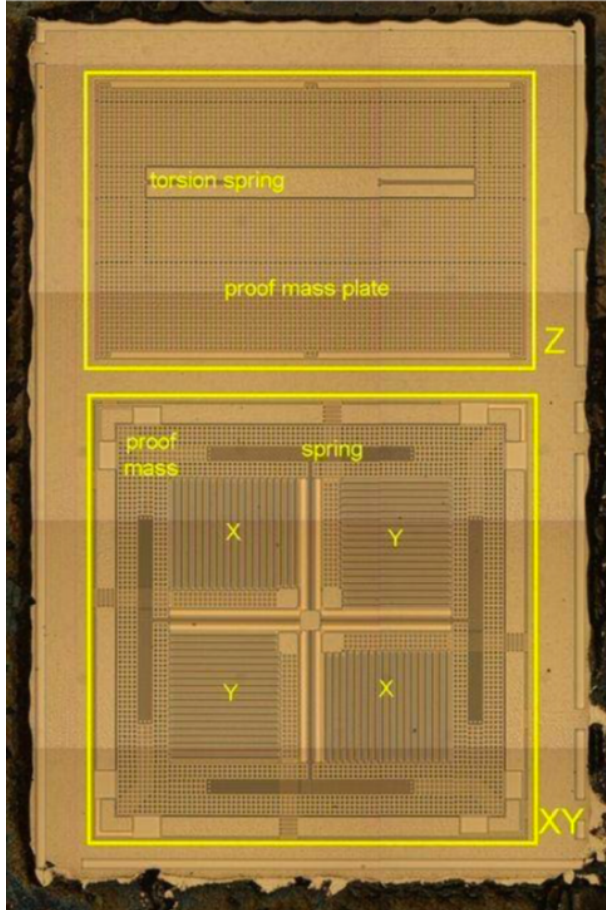


Figure 2: Top view of LIS331DLH [1]

Suspended structures are made fully in epitaxial polysilicon, whose characteristics are the following:

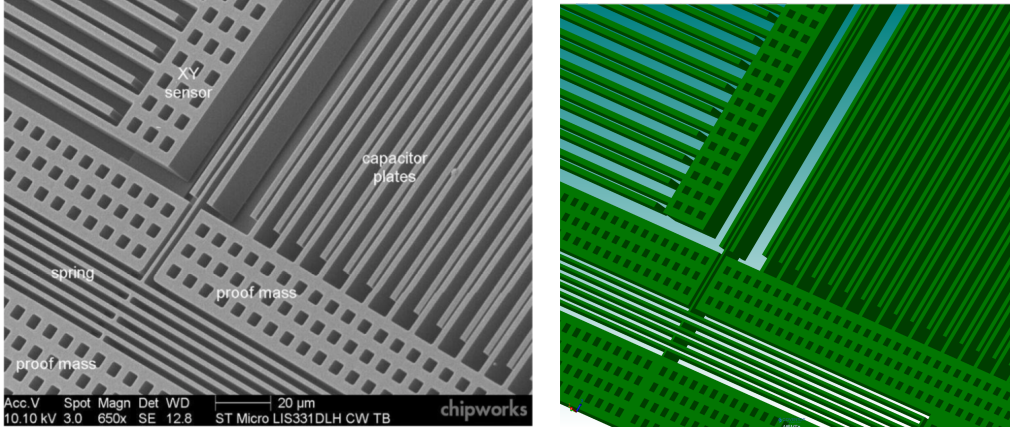


Figure 3: Detailed view with scale of LIS331DLH [1], next to the proposed MEMS+ model

- Young's modulus  $130\text{GPa} < E < 190\text{GPa}$ , most likely  $160\text{GPa}$  even though also  $143\text{GPa}$  was found [5].
- Poisson's ratio  $0.2 < \nu < 0.3$ .
- Density  $\rho = 2320 \text{ kg/m}^3$ .

From reference [3], we were able to understand some typical values of MEMS sensors built with the same process used for the LIS331DLH, the "THELMA" process, created by ST Microelectronics. Specifically, the thickness of the structural layer and the sacrificial layer where found, and used in our model. It also allowed to get an idea of a typical mass of the proof mass, gap size and lengths.

Parameter	Symbol	Value
Resonator length	$L$	$352 \mu\text{m}$
Resonator thickness	$th$	$1.3 \mu\text{m}$
Nominal gap at rest	$g_0$	$2 \mu\text{m}$
Structure height	$h$	$15 \mu\text{m}$
Main spring length	$\ell$	$320 \mu\text{m}$
Folded spring length	$D$	$273 \mu\text{m}$
Spring thickness	$t$	$1.3 \mu\text{m}$
Proof mass	$m$	$6.12 \times 10^{-9} \text{ kg}$

Figure 4: Dimensions of a compact bi-axial micro machined resonant accelerometer [3]

### 3 Model

The acceleration on the XY plane is detected by means of the motion of a proof mass, which is the perforated frame at the periphery of the structure. The mass is connected, employing four box springs, to a central anchor, which is fixed to the substrate. The motion of the mass in a direction (X or Y) produces the movement of four combs that are attached to it. This is transduced in a change of capacitance between the moving and the fixed beams that form the comb. There are two combs to detect the X motion and two to detect the Y motion, in order to have a differential capacitance variation on both axes.

For the Z axis, in order to use the same plane of X and Y for this detection, a rectangular proof mass is suspended through two torsional springs in an off-centred position, creating a displacement

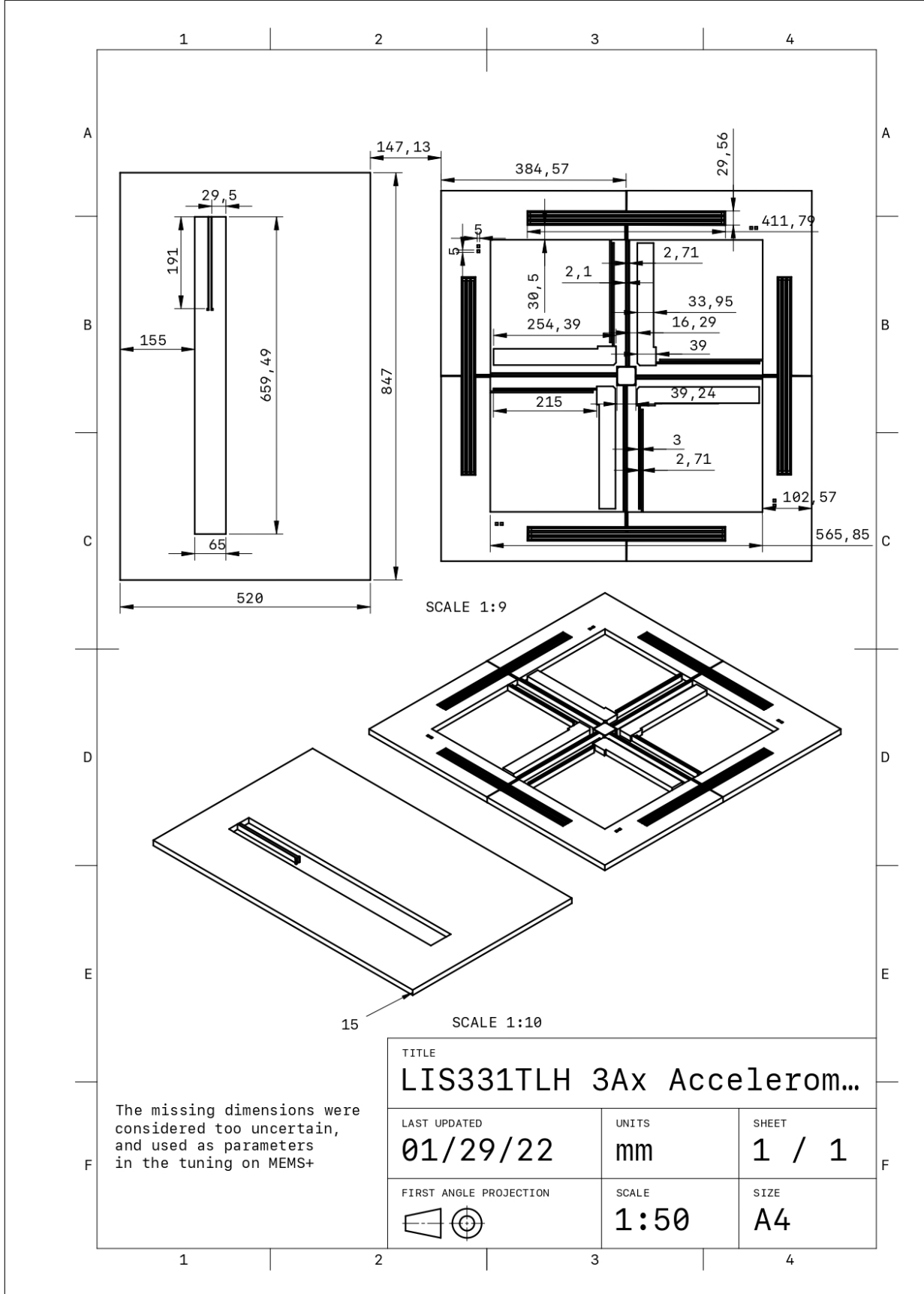


Figure 5: Technical drawing with the final design choices of our model.

due to the torsion and consequently a variation of capacitance by gap closing. From the pictures, it could be noticed that the electrodes below the proof mass are disposed in 2 rectangles, highlighted in figure 6, of equal width, symmetrically placed around the rotation axis. It could be assumed therefore that also this sensor uses a differential capacitance measurement.

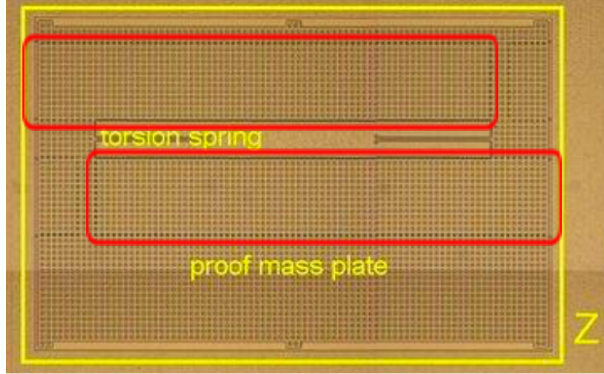


Figure 6: Identification of the electrodes on the z axis sensor

The sacrificial layer used for the fabrication of the MEMS [2], by means of the Thelma process, is composed of two layers, whose total thickness is  $4.1 \mu m$ . This allowed us to know the dimension of the gap in the z direction: the distance from the suspended moving parts and the electrode.

## 4 Tuning and Design

In the process of tuning the accelerometer, and researching the desired performance for it, we minimised the number of parameters to set. In particular, we ended up working on pressure, temperature, gap between the combs, mass, stiffness, and voltage. A variation in any of these parameters leads to several variations in the response and the performance of our 3-axis accelerometer.

- The **pressure** is directly proportional to the damping of the system, and therefore inversely proportional to the quality factor. Moreover, an increase in pressure leads to higher values of noise.  
*Variable: "Pressure" [Pa] in the MEMS+ model*
- The **temperature** influences the system with its proportionality to noise. We decided to perform the analysis on the accelerometer at ambient temperature ( $T = 25C$ ), the same that has been used to collect the results given in the accelerometer's datasheet of STMicroelectronics [4].  
*Variable: "T" [K] in the MEMS+ model*
- The **gap** dimension between the combs is inversely and quadratically proportional to the transduction sensitivity: the smaller the gap, the higher this sensitivity, thus the smaller the acceleration range. In addition, its reduction generates a cubic increase in the squeeze film damping. His minimum dimension is related to the production method, and for the Thelma process it is of  $2\mu m$ .  
*Variable: "Combs.Dist" [\mu m] in the MEMS+ model*
- The **mass** can be varied by changing the dimension and distribution of the holes, since the structure's thickness was defined by the production process and the overall size too complex to change. In particular, the relation between mass and holes dimensions is linear. In particular, we can increase the mass by 3% by decreasing the width of the holes by half a m. Moreover, the configuration of the holes also has a slight effect on the z-axis damping. Finally, a change in the mass brings to different mode frequencies, following the relation  $\omega_0 = \sqrt{\frac{K}{M}}$ . Thus, an increase in the mass generates a reduction of the bandwidth.  
*Variables: "Hole" and "Spac" [\mu m] in the MEMS+ model*

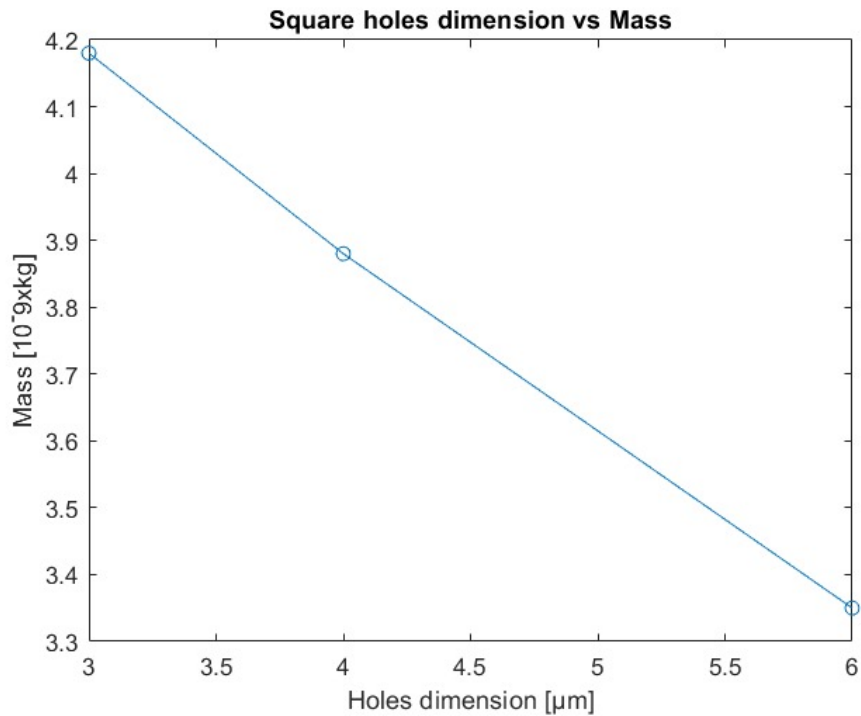


Figure 7: Linear dependence between the dimension of the holes and the mass of the structure

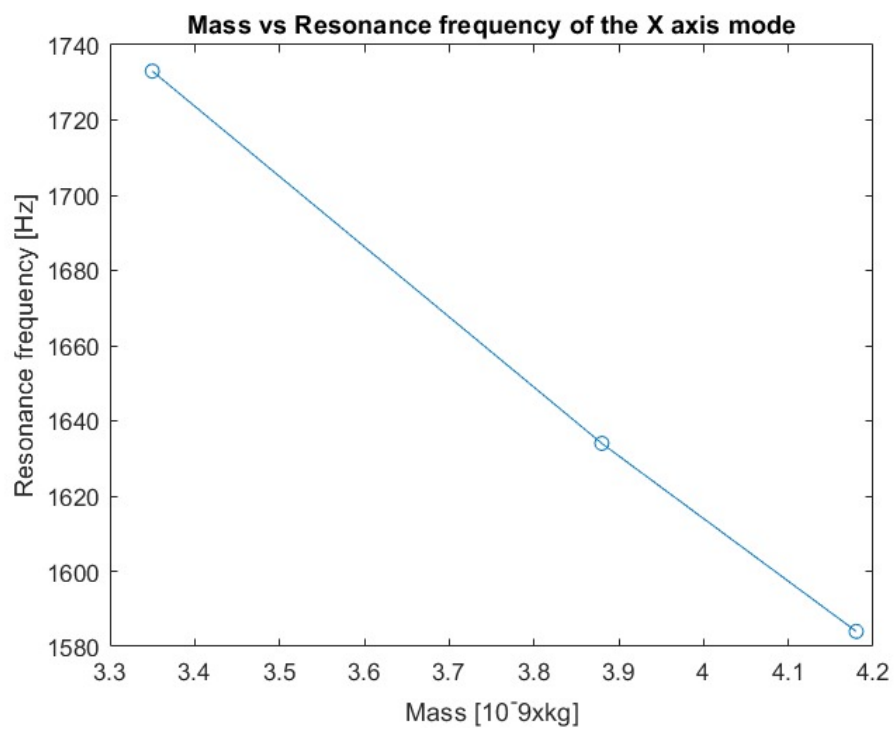


Figure 8: Relation between mass of the structure and natural frequency of the mode along x-axis. For the small interval allowed, the variation is almost linear (approximation of  $\omega \propto M^{-0.5}$ )

- The **stiffness** of the system has the opposite effect on the resonance frequency, compared to the mass. Its value derives from the intrinsic stiffness of the chosen material, thus to its Young's modulus, and from the geometry of the system. Therefore, its value has been controlled mainly through the variation of the X and Y thicknesses of the box spring beams. Finally, by increasing the stiffness of the combs, it is possible to achieve wider values for squeeze film damping the acceleration range.

*Variables: "Torsional.Thick", "BoxSpring.ThickX" and "BoxSpring.ThickY" [ $\mu\text{m}$ ] in the MEMS+ model*

- Adding a **difference of potential** between the stator and the moving combs leads to a reduction of the gap between the combs (eventually reducing it to values lower than the ones achievable by the production method), with consequent increase in sensitivity, damping (due to the squeeze film), and reduction of the range. The system was sized to ensure a range very similar to the one given in the datasheet ( $8g$ ), while maximising the sensitivity and bringing the quality factor the closest to 0.5 possible. The voltage difference can be used to change the measurement range, useful since in the datasheet is said that it can be set by the user on  $2g$ , and  $4g$  just with a different logical input, easily convertible through a DAC into a different voltage setting. The application the sensor under analysis is shown in the following graphs, showing the variance of sensitivity and range with different gap potential (they are not representative of the actual performances achieved).

*Variables: "Voltage.Delta" and "Voltage.DeltaZ" [V] in the MEMS+ model*

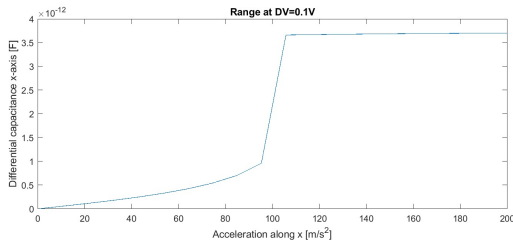


Figure 9: Sensitivity with a potential difference of 0.1 V, along x axis

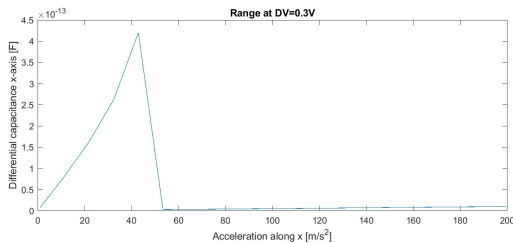


Figure 10: Sensitivity with a potential difference of 0.3 V, along x axis

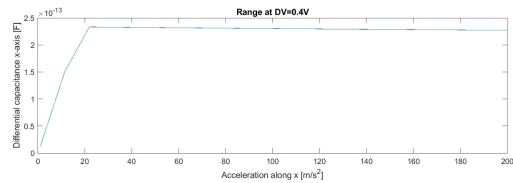


Figure 11: Sensitivity with a potential difference of 0.4 V, along x axis

We started our design process by focusing on three main performance characteristics that we managed to recover: the bandwidth - which should be higher than  $500\text{Hz}$  [4]-, the quality factor - trying to keep its value as close as possible to the optimal value of 0.5 -, and the acceleration range - that should not be lower than  $8g$  [4]-.

In particular, our first goal was to achieve the optimal value of 0.5 for the quality factor, for all the 3 dimensions. However, we immediately noticed that we had important variations in the damping along the z-axis, with respect to the damping along the x and y-axis. Indeed, considering ambient pressure and temperature, the damping in the z-direction was so high that the modal analysis would not show its mode. Hence, we decided to vary the pressure, in order to solve this problem.

One possibility we thought about was to decrease the pressure value only for the z-direction. However, that did not seem particularly feasible from a production point of view.

Therefore, we decreased the pressure until we could have a proper mode identification along the z-direction. In particular, we reached a value of  $10000\text{Pa}$ , which corresponds to a condition of low vacuum, therefore reasonably achievable on the production chain.

Moreover, we decreased the stiffness along the z-direction, in order to achieve a resonance frequency similar to the ones already obtained for the modes along x and y; checking that the desired bandwidth, range, and sensitivity were ensured. As a counter-side effect, we registered an important drop in the damping regarding x and y directions. This led to very high values for the quality factor (around 70). Eventually, we mitigated this problem by reducing stiffness and gap, still trying to keep a distance coherent to the one shown in the photos from [1].

Finally, after having found - and fixed - reliable values for mass, gap, and pressure, we came to a final trade-off: we had to accept quite high values for the quality factor in x and y (around 12), having resonance frequencies big enough to ensure linearity over the bandwidth of  $500\text{Hz}$ .

We only had a few possibilities to decrease Q in those directions.

The first was to decrease the gap between the combs, increasing the squeeze film damping. However, it would have led to values of sensitivity around  $200\text{fF/g}$  for x and y, extremely higher than the one along z ( $3\text{fF/g}$ ), it furthermore was visually very different from the photos available, over than non achievable by the Thelma process.

Secondly, Damping could be increased by increasing the pressure, but in doing so the damping on the Z axis, already lower than 0.5, would have increased. Its mass could be just slightly increased by changing the holes dimensions, and its stiffness, if increased, would have led to a further reduction of the sensitivity, as the gap (corresponding to the sacrificial layer thickness) was fixed by the production method. Lowering further the Q factor along z would have led to a loss of linearity on the desired bandwidth.

Regarding decrements of mass on the x-y proof mass, only minor results could be accomplished via the holes, and being the relationship with the quality factor radical, it would have brought minor improvements. A stiffness increment was limited by the consequent increment of resonance frequency, already very high, and reduction of sensibility.

The second was to modify the Rayleigh damping parameters, to increase the damping in the system. Still, we did not find any reliable data for  $\alpha$  and  $\beta$  from the literature, for our material. Moreover, it would have led to lower bandwidth. Thus, we just used the values of the gyroscope's lab ( $\alpha = 0$  and  $\beta = 1e - 10$ ).

After a countless number of iterations, mostly playing with pressure, thicknesses and voltages, an optimum seemed to be achieved, at the cost of a slightly high quality factor, while giving the expected performances. The final values are reported in the next section, together with the performance evaluation.

## 5 Results and Conclusion

Finally, the analysis gave us the following graphics and results. In table 5, the quality factor, frequencies and Sensitivity on the 3 axis can be seen. The Stator had a voltage of  $2.5\text{ V}$ , as of datasheet, while the x-y proof mass is at  $0.7\text{V}$ . The pressure is  $10\text{kPa}$  (0.1 Atm), the gap between the combs  $2\mu\text{m}$ ,

	Frequency [Hz]	Quality factor	Sensitivity [fF/g]
Mode #3 (X axis)	2471	3.40	14.3
Mode #4 (Y axis)	273	3.40	14.7
Mode #2 (Z axis)	1437	0.50	1.7
Only a cross axis sensitivity between X & Y			0.2

the minimum achievable with the Thelma process. The XY proof mass weight  $5.25\mu g$ , while the Z proof mass weight  $9.16\mu g$ . The Bode plots of figure 12 help showing the achieved linearity over the bandwidth required, until circa 500.

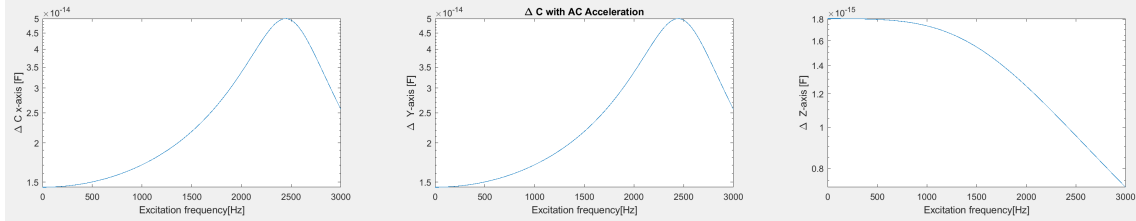


Figure 12: Bode plots of the responses on the three axis

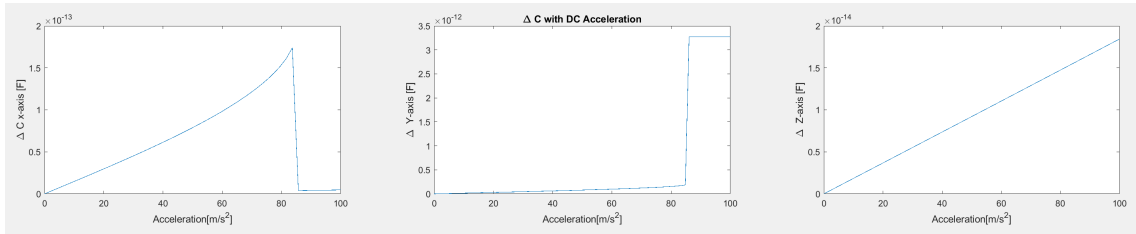


Figure 13: Measurement ranges on the 3 axis

From the graphs in figure 13 it is possible to calculate the maximum acceleration range. Indeed, when the acceleration range's limit of our accelerometer's model is reached, the capacitance drops to zero or saturates, because of the contact between the combs. Thus, the acceleration range in x, y and z is respected. The voltage difference on the x-y sensor is of  $1.8V$ . On the Z sensor the difference of voltage needed to be very big in order to give results, due to the wider gap (related to the sacrificial layer), so it was put to 0.

The noise in the system, shown in figure 14 has an order of magnitude of  $10^{-23}$  for x and y, and  $10^{-22}$  for z, particularly lower than the values of the frequency response, which are around  $10^{-14}$ . These low values of noise are beneficial for the accelerometer, and can be partially addressed to the medium vacuum condition - thus low pressure - of the package, and in general low damping of the system.

Finally, the behaviour with respect to the temperature was evaluated, focusing mostly on the noise. Differences due to the temperature on the sensitivity were not found.

Overall, the results achieved were evaluated satisfying, even if some more analysis and iterations would have led to a better result. Having little information on the expected behaviour, the model design was led by sticking to the few data available and some general knowledge about good MEMS design, but clearly many parameters were left free. A different choice of target (for example aiming at identical resonance frequencies on the 3 axis, or aiming at quality factors of 1/2 for all) would have led to very different results.

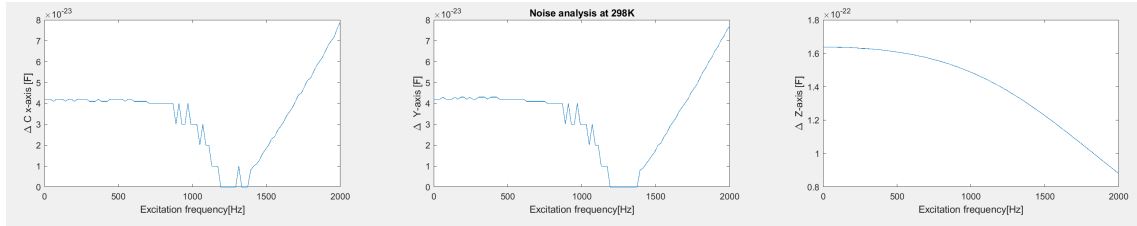


Figure 14: Noise analysis, with no acceleration, at 25C

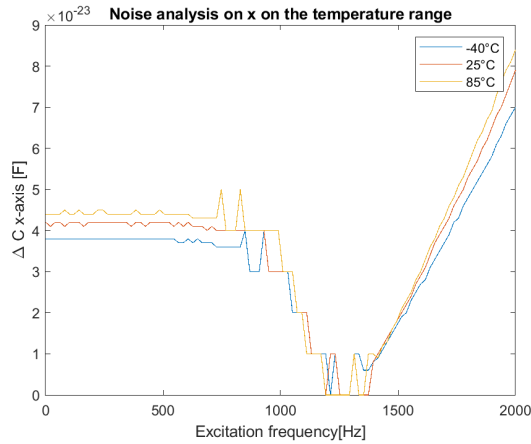


Figure 15: Noise analysis on x axis

## References

- [1] St.J. Dixon-Warren (2010) *MOTION SENSING IN THE IPHONE 4: MEMS ACCELEROMETER*, MEMS Journal, <https://www.memsjournal.com/2010/12/motion-sensing-in-the-iphone-4-mems-accelerometer.html>.
- [2] Corigliano, De Masi, Frangi, Comi, Villa, Marchi (2004) *Mechanical characterization of polysilicon through on-chip tensile tests*, IEEE Xplore, <https://doi.org/10.1109/JMEMS.2003.823221>.
- [3] Caspiani, Comi, Corigliano, Langfelder, Tocchio (2013) *Compact biaxial micromachined resonant accelerometer*, IOP Science, <https://iopscience.iop.org/article/10.1088/0960-1317/23/10/105012>.
- [4] STMicroelectronics *3-axis digital accelerometer, ultra low power operational modes, advanced power saving, smart sleep to wake-up functions*, <https://www.st.com/en/mems-and-sensors/lis331dlh.html>.
- [5] Villa, Masi (2003) *Mechanical characterization of epitaxial polysilicon in MEMS*, <https://doi.org/10.1016/B978-008044046-0.50178-0>.